Consequences of Mechanical and Radiative Feedback from Black Holes in Disc Galaxy Mergers

Ena Choi[1]⋆, Thorsten Naab[2], Jeremiah P. Ostriker[1,3], Peter H. Johansson[4], Benjamin P. Moster[2]

[1] *Department of Astrophysical Sciences, Princeton University, Princeton, NJ 08544, USA*
[2] *Max-Planck-Institut für Astrophysik, Karl-Schwarzschild-Strasse 1, 85741 Garching, Germany*
[3] *Department of Astronomy, Columbia University, New York, NY 10027, USA*
[4] *Department of Physics, University of Helsinki, Gustaf Hällströmin katu 2a, FI-00014 Helsinki, Finland*

arXiv:1308.3719v2 [astro-ph.CO] 10 Mar 2014

ABSTRACT

We study the effect of AGN mechanical and radiation feedback on the formation of bulge dominated galaxies via mergers of disc galaxies. The merging galaxies have mass-ratios of 1:1 to 6:1 and include pre-existing hot gaseous halos to properly account for the global impact of AGN feedback. Using smoothed particle hydrodynamics simulation code (GADGET-3) we compare three models with different AGN feedback models: (1) no black hole and no AGN feedback; (2) thermal AGN feedback; and (3) mechanical and radiative AGN feedback. The last model is motivated by observations of broad absorption line quasars which show winds with initial velocities of $v_{\mathrm{w}} \geqslant$ 10,000 km s^{-1} and also heating associated with the central AGN X-ray radiation. The primary changes in gas properties due to mechanical AGN feedback are lower thermal X-ray luminosity from the final galaxy - in better agreement with observations - and galactic outflows with higher velocity $\sim$ 1000 km s^{-1} similar to recent direct observations of nearby merger remnants. The kinetic energy of the outflowing gas is a factor of $\sim$ 20 higher than in the thermal feedback case. All merger remnants with momentum-based AGN feedback with $v_{\mathrm{w}} \sim 10,000$ km s^{-1} and $\epsilon_{\mathrm{f}} = 2 \times 10^{-3}$, independent of their progenitor mass-ratios, reproduce the observed relations between stellar velocity dispersion and black hole mass ($M_{\mathrm{BH}} - \sigma$) as well as X-ray luminosity ($L_X - \sigma$) with $10^{37.5} \lesssim L_X(0.3 - 8 \text{ keV})/\text{erg s}^{-1} \lesssim 10^{39.2}$ for velocity dispersions in the range of 120 km s$^{-1} \lesssim \sigma \lesssim$ 190 km s^{-1}. In addition, the mechanical feedback produces a much greater AGN variability. We also show that gas is more rapidly and impulsively stripped from the galactic centres driving a moderate increase in galaxy size and decrease in central density with the mechanical AGN feedback model.

Key words: accretion, accretion discs – black hole physics – galaxies: active– galaxies: nuclei – galaxies: formation – quasars: general

1 INTRODUCTION

Accretion onto central massive black holes in galactic nuclei emits energy in the form of electromagnetic radiation, relativistic jets, and wider angle non-relativistic outflows (Lynden-Bell 1969; Rees 1984). The coupling of the energy output to the gas in galaxies, i.e. active galactic nucleus (AGN) feedback, is believed to play an important role in galaxy formation by regulating central star formation and quenching cooling flows and produce approximately the linear relationship between

the central massive black hole and the stellar component of the elliptical galaxy (Dressler 1989; Kormendy 1993; Magorrian et al. 1998; Gebhardt et al. 2000; Tremaine et al. 2002; Marconi & Hunt 2003; Aller & Richstone 2007; Gültekin et al. 2009). However, understanding the precise physical mechanisms by which this feedback occurs poses a major challenge for our understanding of the connection between AGN physics and galaxy evolution. Several mechanisms have been proposed and numerically investigated, including radiative heating (Sazonov et al. 2005; Ciotti & Ostriker 2007; Ciotti, Ostriker & Proga 2009), radiation pressure (Debuhr et al. 2010), cavities generated by the injection of thermal energy or cosmic

⋆ E-mail:echoi@astro.princeton.edu

rays (Dalla Vecchia et al. 2004; Sijacki et al. 2007, 2008; Guo & Mathews 2010; Broderick, Chang & Pfrommer 2012; Pfrommer, Chang & Broderick 2012; Puchwein & Springel 2013), thermal energy input (Di Matteo, Springel & Hernquist 2005; Springel 2005) or bipolar mechanical outflows and jets (Omma et al. 2004; Nayakshin & Power 2010; Kim et al. 2011; Debuhr, Quataert & Ma 2012; Choi et al. 2012; Gaspari, Brighenti & Temi 2012; Gaspari, Brighenti & Ruszkowski 2013; Barai et al. 2014).

Based on one- and two- dimensional computations, Ostriker et al. (2010) quantitatively studied the relative importance of the different processes in protecting the central black hole from excessive mass growth and found mechanical feedback with proper mass and momentum injection to be the dominant mode of feedback. Energy deposition from a central AGN feedback takes place when the accretion rates onto the central black hole are high, e.g. when the density of the surrounding gas is high. If the cooling time of the gas is resolved and is sufficiently short, the gas tends to instantly radiate away any thermal energy input. Therefore, thermal energy input is a rather inefficient regulator for black hole growth. Recently Dalla Vecchia & Schaye (2012) pointed out that the thermal AGN feedback implemented with the multiphase star-formation model (Springel & Hernquist 2003) has negligible effect since the energy deposited to star-forming gas particles is radiated away quickly. Barai et al. (2014) further confirmed this showing more limited effect of thermal feedback with the expansion of the artificial hole around black hole limited. On the other hand, momentum input, which cannot be radiated away easily, was found to be very efficient in limiting the infall and accretion onto the central black hole in one- and two- dimensional simulations (Ostriker et al. 2010). It also tends to impart considerably more kinetic energy to the outflowing gas at a given accretion rate and efficiency of energy release.

In this context, Choi et al. (2012) hereafter CONJ12, introduced and tested the modeling of mechanical feedback from AGN communicating to the ambient gas via a bipolar wind in three-dimensional smoothed particle hydrodynamical (SPH) simulations to verify whether this form of feedback is able to regulate black hole growth. This treatment also includes a modified algorithm for the black hole accretion rate with a Bondi radius criterion and the effect of radiation from the accreting black hole. We used simulations of isolated discs and of one equal-mass disc merger to demonstrate that massive, non-relativistic outflows can indeed regulate the black hole growth. Also, the new treatment of the AGN feedback results in stronger outflows at higher velocity (up to $v_{\rm w} \sim 2,000$ km s^{-1}), a greater fluctuation level in both the radiant and wind outflow rates, and lower X-ray luminosities of hot gas compared to the thermal feedback treatment that is commonly adopted in many three-dimensional hydrodynamic calculations (e.g., Springel, Di Matteo & Hernquist 2005a,b; Di Matteo, Springel & Hernquist 2005; Hopkins et al. 2005; Sijacki et al. 2007; Sijacki, Springel & Haehnelt 2009; Booth & Schaye 2009; Johansson, Naab & Burkert 2009; Teyssier et al. 2011; Dubois et al. 2012; Newton & Kay 2013).

In this paper we extend our previous work and study the effect of radiation and strong winds from AGN on the gas as well as the stellar component of the host galaxies during mergers of equal- and unequal-mass disc galaxies. These merging disc galaxies now include an extended hot gaseous halo (Moster et al. 2011) as predicted by cosmological hydrodynamical simulations of galaxy formation (Toft et al. 2002; Crain et al. 2010, 2013), and as inferred from X-ray observations of normal massive disc galaxies (e.g. Anderson & Bregman 2011; Anderson, Bregman & Dai 2013; Li & Wang 2013). Such a component was neglected in previous AGN feedback studies using idealized simulations. It is, however, most relevant for a proper treatment of the hydrodynamic interaction of the AGN wind with the ambient medium and for a more accurate determination of the X-ray properties.

We further study the effect of mechanical AGN feedback on the evolution of the stellar component of the host galaxy. During active phases of the black hole large amounts of gas can be removed from the central regions of the galaxies on short timescales. It has been argued that this process can trigger a significant dynamical expansion of the stellar component (Fan et al. 2008, 2010; Hopkins et al. 2010; Martizzi et al. 2012; Dubois et al. 2013). This process might be relevant in the context of recent observational studies indicating that many massive, passively evolving galaxies at high redshift ($z > 1$) are more compact than local galaxies with the same stellar mass (Ferguson et al. 2004; Trujillo et al. 2004; Longhetti et al. 2007; Toft et al. 2007; Trujillo et al. 2007; Cimatti et al. 2008; van Dokkum et al. 2008; Damjanov et al. 2009). While much of the mass growth and corresponding size growth in the outer parts of giant ellipticals is potentially driven by accretion of stars in minor mergers (Oser et al. 2012; Johansson, Naab & Ostriker 2012; Hilz et al. 2012; Oogi & Habe 2013; Hilz, Naab & Ostriker 2013; Bédorf & Portegies Zwart 2013, but see Newman et al. 2012; Nipoti et al. 2012). Observations by van Dokkum et al. (2008); Szomoru et al. (2010); Saracco, Gargiulo & Longhetti (2012); van de Sande et al. (2013) and others also indicate a decrease in central densities which does not easily occur in the minor merger picture (cf. Hilz, Naab & Ostriker 2013). These observations suggest that in addition to merging an additional mechanism is needed. We test the contribution of the AGN driven wind to the galaxy size growth and the central density decrease.

The paper is organized as follows. In Section 2, we provide a brief summary of the simulation code and the initial conditions. We also summarize the algorithmic implementation of the black hole accretion and feedback model. We present our result for the equal- and unequal-mass merger simulations in Section 3 with a detailed analysis of the effect of the assumed feedback model ('mechanical' vs. 'thermal') and the progenitor mass-ratio on star formation, black hole growth growth and the properties of the AGN driven wind. In Section 4 we discuss the impact of mechanical and thermal feedback on the properties of the merger remnant and highlight the effect on the X-ray luminosities as well as the size and central density of the stellar component. We also discuss the black hole and X-ray scaling relations. Finally, in Section 5 we summarize and discuss our main results.

2   METHODOLOGY

2.1   Numerical Code

We perform the simulations using the parallel TreeSPH-code GADGET-3 (Springel 2005). The code employs the Lagrangian SPH (see Monaghan 1992) technique for gas particles and solves the equations of motion for the collisionless dark matter and star particles. The sub-resolution modeling for star formation assumes a two-phase medium of hot and cold gas (McKee & Ostriker 1977; Springel & Hernquist 2003), and the stars form from a cold component embedded in sufficiently dense gas, i.e., $n > n_{\rm th} = 0.128$ cm^{-3} with the short-lived stars supplying a thermal energy of 10^{51} erg to the surrounding gas per supernovae (SNe). SN-driven galactic winds are not included in this study. We include the radiative cooling for a primordial composition of hydrogen and helium (Katz, Weinberg & Hernquist 1996) and a spatially uniform time-independent UV background radiation field with a modified Haardt & Madau (1996) spectrum. The dimensionless Hubble parameter is $h = 0.71$ such that the present-day Hubble parameter is $H_0 = 71$ km s^{-1} Mpc^{-1}.

2.2   Initial conditions and galaxy parameters

We simulate binary mergers of equal and unequal mass and the initial galaxy disc galaxy models are constructed following Springel, Di Matteo & Hernquist (2005b). We additionally include a diffuse, rotating hot gaseous halo as described in Moster et al. (2011, 2012). The progenitor galaxies are composed of a rotationally supported disc of gas and stars, a stellar bulge and a central black hole embedded in a halo consisting of hot gas and dark matter. Each galaxy has a virial velocity and radius $v_{\rm vir} = 160$ km s^{-1}, and $r_{\rm vir} = 160$ h^{-1} kpc corresponding to a virial mass of $M_{\rm vir} = 9.53 \times 10^{11}$ $h^{-1} M_\odot$. The Hernquist (1990) profile dark matter halos are constructed with a concentration parameter $c = 9$ of the corresponding Navarro–Frenk–White (NRW) halo (Navarro, Frenk & White 1995). The dark matter halo is then populated with exponential discs with a baryonic mass fraction of $m_d = 0.041$, with a gas fraction of $f_{\rm gas} = 0.2$ and with the rest being stars. We set the disc scale length r_d using the Mo, Mao & White (1998) formalism, assuming that the fractional disc angular momentum equals the disc mass fraction m_d for a constant halo spin of $\lambda = 0.033$ for all models. The vertical scale height z_0 of the stellar disc is radially constant and set to $0.2 r_d$. The black hole at the centre of each galaxy is modeled as a collisionless sink particle which can accrete gas and the initial seed black hole masses is $10^6 M_\odot$.

We model the hot gaseous component as a slowly rotating halo with a spherical density profile. The density distribution follows the observationallymotivated beta-profile (Cavaliere & Fusco-Femiano 1976; Jones & Forman 1984; Eke, Navarro & Frenk 1998). It has three free parameters: the central density ρ_0, the core radius r_c and the outer slope parameter beta. We adopt $\beta = 2/3$ (Jones & Forman 1984), $r_c = 0.22 r_s$ (Makino, Sasaki & Suto 1998) and fix ρ_0 such that the hot gas mass within the virialradius is $M_{gas,halo}$. The hot gaseous halo is rotating around the spin axis of the disc. The angular momentum of the hot gaseous halo

Table 1. Orbital Parameters of Initial Condition

Mass Ratio	$R_{\rm init}$[a]	$r_{\rm peri}$[b]
1:1	160.0	5.0
2:1	143.5	4.45
3:1	135.0	4.2
6:1	124.0	3.8

[a] The initial separation of the progenitors
[b] The pericentric distance of the progenitors

is set by requiring that the specific angular momentum of the the the gas. $j_{\rm gas,halo} = J_{\rm gas,halo}/M_{\rm gas,halo}$ is a multiple of the specific angular momentum of the dark matter halo $j_{\rm DM} = J_{\rm DM}/M_{\rm DM}$ such that $j_{\rm gas,halo} = a j_{\rm DM}$. A value of $a = 1$ matches the commonly adopted assumption that there is no angular momentum transport between the dark matter halo and the gaseous halo. The angular momentum distribution is then assumed to scale with the product of the cylindrical distance from the spin axis R and the circular velocity at this distance: $j(R) \propto R\, v_{\rm circ}(R)$. The vertical velocity of the gas halo particles is set equal to be zero.

We set the orbital geometry to be G13 (Naab & Burkert 2003) for our merger simulation following Johansson, Naab & Burkert (2009). This geometry corresponds to the inclinations $i_p = -109, i_s = 180$ and the arguments of pericenter $\omega_p = 60, \omega_s = 0$ for the primary and secondary galaxies, respectively. The galaxies approach each other on parabolic orbits. The initial separation of the progenitors of the 1:1 mergers is $R_{\rm init} = r_{\rm vir}$ with a pericentric distance of $r_{\rm peri} = 2 r_{\rm d}$, where $r_{\rm vir} = 160 h^{-1}$ kpc is the virial radius and $r_{\rm d} = 2.5$ h^{-1}kpc is the disc scale length. For the unequal-mass mergers the initial separation is the mean of the virial radii of the two galaxies. The pericentric distance is $r_{\rm peri} = 2 r_{\rm d,mean}$, the mean disc scale radius of the two progenitors (see Table 1 for details). Every simulation was evolved for a total of $t = 3$ Gyr with the merger taking place at around $t \sim 1.5 - 2.0$ Gyr.

For all simulations, the primary galaxy is realized with 1.7×10^6 particles: the halo has 8.0×10^5 dark matter particles and 1.3×10^5 gas particles, the disc has 4.8×10^5 stellar particles and 1.2×10^5 gas particles, and the bulge has 2.0×10^5 stellar particles. For the secondary galaxies in minor mergers, we scale down the galaxy masses and particle resolution accordingly in order to maintain equal mass resolution. The smaller galaxy in a 2:1 merger, for example, has half the number of particles than the more massive galaxy (See Table 2). All gas and star particles have the same mass of $m_{*,\rm gas} = 6.5 \times 10^4$ $M_\odot h^{-1}$ (we spawn one star particle per gas particle), whereas the dark matter particles have a mass of $m_{\rm DM} = 1.1 \times 10^6$ $M_\odot h^{-1}$. The gravitational force softening length is $\epsilon = 66$ pc for the dark matter particles and $\epsilon = 16$ pc for the gas and star particles respectively. We also perform a resolution study, with twice the mass resolution for the fiducial model with the softening length $\epsilon = 52$ pc for the dark matter particles and $\epsilon = 13$ pc for the baryonic particle scaled with the square root of the mass ratio following Dehnen (2001). The simulation parameters are summarized in Table 2.

Table 2. Galaxy Initial Conditions

Model	M_{DM}[a] $M_\odot h^{-1}$	$M_{\mathrm{gas,halo}}$[b] $M_\odot h^{-1}$	$M_{\mathrm{gas,disc}}$[c] $M_\odot h^{-1}$	$M_{*,\mathrm{disc}}$[d] $M_\odot h^{-1}$	$M_{*,\mathrm{bulge}}$[e] $M_\odot h^{-1}$	m_{DM}[f] $M_\odot h^{-1}$	$m_{*,\mathrm{gas}}$[g] $M_\odot h^{-1}$
Half-mass Progenitor	4.4×10^{11}	4.2×10^{9}	3.9×10^{9}	1.6×10^{10}	6.5×10^{9}	1.1×10^{6}	6.5×10^{4}
Fiducial Galaxy	8.8×10^{11}	8.5×10^{9}	7.8×10^{9}	3.1×10^{10}	1.3×10^{10}	1.1×10^{6}	6.5×10^{4}
High Resolution	8.8×10^{11}	8.5×10^{9}	7.8×10^{9}	3.1×10^{10}	1.3×10^{10}	5.5×10^{5}	3.3×10^{4}

[a] dark matter mass, [b] gas mass in halo, [c] gas mass in disc, [d] stellar disc mass, [e] stellar bulge mass, [f] dark matter particle mass, and [g] stellar and gas particle mass.

2.3 The traditional thermal black hole feedback model

In the widely adopted thermal black hole feedback models (e.g. Springel, Di Matteo & Hernquist 2005b), the sub-grid accretion rate on scales smaller than the resolution is estimated with a Bondi-Hoyle-Lyttleton parameterization (Hoyle & Lyttleton 1939; Bondi & Hoyle 1944; Bondi 1952). For gas with density ρ, sound speed c_{s} and velocity relative to the black hole v, the mass accretion rate onto the central region is given as:

$$\dot{M}_{\mathrm{B}} = \frac{4\pi\alpha G^2 M_{\mathrm{BH}}^2 \rho}{(c_{\mathrm{s}}^2 + v^2)^{3/2}}, \qquad (1)$$

where α is a dimensionless parameter, which should be set to unity as long as we resolve the physics and scales related to the Bondi accretion. In the framework of multiphase interstellar medium, however, the accretion rate may be higher than the Bondi accretion rate calculated for star forming gas due to the unresolved cold phase as noted in (Booth & Schaye 2011; Gaspari, Ruszkowski & Oh 2013). We therefore use $\alpha = 32$ in this work, as adopted in CONJ12.

It is assumed that the accretion is limited to the Eddington rate given by

$$\dot{M}_{\mathrm{edd}} \equiv \frac{4\pi G M_{\mathrm{BH}} m_{\mathrm{p}}}{\epsilon_{\mathrm{r}} \sigma_{\mathrm{T}} c}. \qquad (2)$$

Here m_{p} is the proton mass, σ_{T} is the Thomson cross-section and ϵ_{r} is the radiative efficiency assumed to be a fixed value of 0.1, adopted from the mean value for radiatively efficient Shakura & Sunyaev (1973) accretion onto a Schwarzschild black hole. The accretion rate in the standard models is then $\dot{M}_{\mathrm{acc}} = \min(\dot{M}_{\mathrm{B}}, \dot{M}_{\mathrm{edd}})$ with no additional requirement that accreted particles be gravitationally bound to the central black hole.

In the thermal feedback model (e.g. Springel, Di Matteo & Hernquist 2005b; Di Matteo, Springel & Hernquist 2005; Sijacki et al. 2007; Johansson, Burkert & Naab 2009), the feedback energy from the black hole E_{feed} has typically been assumed to be some fraction ϵ_{f} of the rest mass energy of the accreted matter and couples thermally and isotropically to the surrounding gas as,

$$\dot{E}_{\mathrm{feed}} = \epsilon_{\mathrm{f}} \dot{M}_{\mathrm{inf}} c^2. \qquad (3)$$

A fixed value of $\epsilon_{\mathrm{f}} = 0.005$ is adopted in many previous studies (Springel, Di Matteo & Hernquist 2005b; Sijacki et al. 2007), so that 0.5 percent of the total accreted rest mass energy is available as thermal energy which is distributed to

the neighboring ~ 64 gas particles weighted by the SPH kernel. In this approach, neither mass nor momentum is added to the ambient fluid by the black hole and all accretion energy is added via thermal energy.

2.4 The new mechanical black hole feedback model

For the simulations with mechanical feedback from the AGN we use the model presented in CONJ12 which is briefly reviewed in this section. We first calculate the rate of the mass infall onto the black hole with an "alternative averaging (AA)" method using:

$$\dot{M}_{\mathrm{inf,AA}} = \left\langle \frac{4\pi\alpha G^2 M_{\mathrm{BH}}^2 \rho}{(c_{\mathrm{s}}^2 + v^2)^{3/2}} \right\rangle, \qquad (4)$$

where angle brackets denote the averaging over the SPH kernel. This method for the calculation of the black hole mass does the calculation in both time and space on an individual particle basis and then averages the results over the neighboring 64 particles in order to reduce the dependency on the number of SPH particles.

To avoid the unphysical accretion of unbound gas from outside the Bondi radius we statistically limit the accretion of mass to the gas within the Bondi radius. Since the mass distribution of each gas particle is smoothed with the kernel size, we allow for the full accretion rate only if the total volume of a gas particle resides within the Bondi radius. Otherwise, we reduce the probability of being absorbed by the black hole (soft Bondi radius criterion (SB), see CONJ12). To account for the time that it takes a particle at radius r_j to be accreted, we include the free-fall modification (FF) to the accretion probability with an extra factor of

$$p_{j,\mathrm{ff}} = \frac{\frac{1}{\tau_j}}{\frac{1}{N_{\mathrm{sph}}} \sum_{j=1}^{N_{\mathrm{sph}}} \frac{1}{\tau_j}}, \qquad (5)$$

where $\tau_j = r_j/(c_{\mathrm{s},j}^2 + v_j^2)^{1/2}$ is the free fall time and N_{sph} denotes the typical number of smoothing neighboring gas particles of the black hole. For a full description of the soft Bondi radius criterion and the free-fall modification, see Figure 1 and section 2.4 of CONJ12.

Motivated by observations of broad absorption line winds, which convey energy, mass and momentum into the surrounding gas with velocity $\sim 10,000$ km s^{-1} outflows corresponding to a typical broad line wind velocity (Crenshaw, Kraemer & George 2003; Moe et al. 2009; Dunn et al. 2010), we included these observed AGN winds

in our numerical treatment following Ostriker et al. (2010). In our model, the AGN winds carry a mass given by:

$$\dot{M}_{\mathrm{outf}} = \dot{M}_{\mathrm{inf}} - \dot{M}_{\mathrm{acc}}, \qquad (6)$$

where $\dot{M}_{\mathrm{outf}}$, $\dot{M}_{\mathrm{inf}}$ and $\dot{M}_{\mathrm{acc}}$ respectively denote the outflowing/inflowing mass rate and the mass rate actually accreted onto the black hole. For simplicity we assume that the wind is launched at a fixed speed $v_{\mathrm{w}} = 10,000$ km s^{-1}. Then a momentum flux carried by the wind is given as,

$$\dot{p} = \dot{M}_{\mathrm{outf}} v_{\mathrm{w}}, \qquad (7)$$

and the kinetic energy rate of the outflow is given as,

$$\dot{E}_{\mathrm{w}} \equiv \epsilon_{\mathrm{f}} \dot{M}_{\mathrm{acc}} c^2, \qquad (8a)$$
$$= \frac{1}{2} \dot{M}_{\mathrm{outf}} v_{\mathrm{w}}^2, \qquad (8b)$$

where ϵ_{f} denotes the feedback efficiency. We can define the dimensionless quantity ψ, the ratio of the mass outflow rate to the accreted rate as,

$$\psi \equiv 2\epsilon_{\mathrm{f}} c^2 / v_{\mathrm{w}}^2 = \dot{M}_{\mathrm{outf}} / \dot{M}_{\mathrm{acc}}, \qquad (9)$$

and we can rewrite the equation for the black hole accretion rate as,

$$\dot{M}_{\mathrm{acc}} = \dot{M}_{\mathrm{inf}} \frac{1}{1 + \psi}. \qquad (10)$$

As discussed in Ostriker et al. (2010) and CONJ12, in the presence of significant AGN winds, not all of the mass entering the central region $\dot{M}_{\mathrm{inf}}$ actually reaches the black hole. For example, with the feedback efficiency typically adopted in the literature, $\epsilon_{\mathrm{f}} = 0.005$, and with the fixed wind velocity $v_{\mathrm{w}} = 10,000$ km s^{-1}, only 10 percent of the inflowing mass is actually accreted onto the black hole while 90 percent is ejected in a wind.

We calculate the dimensionless quantity ψ for the given feedback efficiency ϵ_{f} and wind velocity v_{w}, and stochastically select the wind particles from all gas particle attracted into the central zone by the black hole keeping the fraction of wind particles to the total inflowing particles as $\psi/(1+\psi)$. To deposit the wind mass and momentum, we give kicks to the gas particles selected following the stochastic approach. We set the direction of the wind to be parallel or anti-parallel to the direction of angular momentum of each gas particle, if the central black holes are surrounded by a gas disc this procedure results in a wind perpendicular to the disc plane (Proga & Kallman 2004). The emitted wind particles share their momentum with two other nearby gas particles to reproduce the shock heated momentum-driven flows. We deposit the residual energy into these three particles in thermal form so that the total energy is conserved. Having momentum share starts the cascade with twice the number of particles and it makes it approach the Sedov solution faster, and makes us less subject to the problem of having not enough resolution to correctly represent a hydrodynamic outflow.

In addition to the mechanical feedback described above, X-ray radiation from the accreting black hole can be coupled to the surrounding gas according to an approximation described in Sazonov et al. (2005), as in Ciotti, Ostriker & Proga (2010); Novak, Ostriker & Ciotti (2011); CONJ12. The luminosity flux from the two black holes is calculated at the position of each gas particle, and the flux is converted to the net volume heating rate $\dot{E}$ by

adopting the Sazonov et al. (2005) formulae that include Compton heating and photoionization heating. Note that Equation 10, not Equation 4, determines the AGN luminosity flux and thus the magnitude of the radiation feedback. We also include the electromagnetic momentum, the radiation pressure from the X-ray flux from the black hole by adding a momentum per unit time of $\dot{p} = \dot{E}/c$. The added force is directed radially away from the black holes.

Finally, instead of limiting the maximum accretion rate to the Eddington rate (Equation 2), we compute the Eddington force acting on the surrounding gas particles, directed radially away from the black hole as described in CONJ12 and allow this force to act on the gas flow through the hydrodynamic equations. Naturally it reduces the inflow and increases the outflow but accretion exceeding the Eddington rates can occasionally occur.

3 COMPARISON OF THERMAL AND MECHANICAL FEEDBACK MODELS

We explore the effects of AGN feedback with three types of simulations: no black hole and AGN feedback (No-AGN); thermal AGN feedback (Th-AGN); and momentum-based mechanical and radiation AGN feedback with X-ray heating and radiation pressure (MR-AGN). All equal and unequal-mass mergers are run with identical merger orbits and initial disc orientations. The simulated final black hole properties and galaxy remnant properties are given in Table 3 and 4, respectively. Note that we use the model for modified black hole mass accretion (Section 2.4) only for the MR-AGN models, the momentum-based mechanical AGN feedback. For Th-AGN models we use the standard mass accretion prescription and parameters adopted and studied in the previous studies (e.g. Di Matteo, Springel & Hernquist 2005) which produce a broad agreement with observational constraints. The number following the model acronyms indicates the assumed feedback efficiency in units of 10^{-4}, i.e. Th-AGN-50 is the thermal feedback model with a feedback efficiency of $\epsilon_{\mathrm{f}} = 5 \times 10^{-3}$; MR-AGN-05 is the mechanical feedback model with a feedback efficiency of $\epsilon_{\mathrm{f}} = 5 \times 10^{-4}$ (see Table 3). The model Th-AGN-50 is identical to the black hole accretion and AGN feedback model described in Springel, Di Matteo & Hernquist (2005b).

3.1 Black hole growth and star formation rate

Figure 1 shows the global star formation rate, the net accretion rate onto the black hole, the Eddington ratio of the mass accretion ($\dot{M}_{\mathrm{acc}}/\dot{M}_{\mathrm{Edd}}$) and the evolution of the black hole mass (summed over both black holes prior to merging) for the three different feedback models: No-AGN (black curve), Th-AGN-50 (e.g., Springel, Di Matteo & Hernquist 2005b, blue curves), and MR-AGN-20 (red curves). Note that the thermal feedback model Th-AGN-50 adopts a feedback energy coupling efficiency of $\epsilon_{\mathrm{f}} = 5 \times 10^{-3}$, the value adopted in Springel, Di Matteo & Hernquist (2005b) and the MR-AGN-20 adopts $\epsilon_{\mathrm{f}} = 2 \times 10^{-3}$. We decided to compare these two models as they result in merger remnants with comparable final black hole mass. We additionally show the control run only with the mechanical feedback, M-AGN-20 (orange

Table 3. The simulated merger sample: black hole properties

Model	Mass Ratio	$\epsilon_f{}^a$	$\log M_{\rm BH,f}$ $M_\odot$	$l_{\max}^{\rm BH,eff}{}^b$	$l_{\min}^{\rm BH,eff}$	$\sigma_{\rm fluc}{}^c$	$\log E_{\rm BH}{}^d$ erg
(1)	(2)	(3)	(4)	(5)	(6)	(7)	(8)
No-AGN	1:1	-	-	-	-	-	-
Th-AGN-50^e	1:1	5×10^{-3}	8.14	-0.70	-5.98	0.27	60.09
Th-AGN-20	1:1	1×10^{-3}	8.42	-0.70	-4.66	0.25	59.98
Th-AGN-05	1:1	5×10^{-4}	8.73	-0.70	-5.44	0.18	59.69
MR-AGN-50	1:1	5×10^{-3}	7.83	0.70	-4.30	6.00	59.79
MR-AGN-20^f	1:1	2×10^{-3}	8.30	1.18	-6.11	4.77	59.86
M-AGN-20^g	1:1	2×10^{-3}	8.40	1.58	-6.51	4.80	59.96
MR-AGN-05	1:1	5×10^{-4}	9.03	1.25	-4.37	4.90	59.98
High-MR-AGN-20^h	1:1	2×10^{-3}	8.26	1.16	-4.91	4.82	59.82
Th-AGN-50-2:1	2:1	5×10^{-3}	6.94	-0.70	-3.98	0.20	58.89
Th-AGN-50-3:1	3:1	5×10^{-3}	6.80	-0.70	-4.54	0.19	58.75
Th-AGN-50-6:1	6:1	5×10^{-3}	6.63	-0.70	-4.04	0.21	58.58
MR-AGN-20-2:1	2:1	2×10^{-3}	7.65	-0.21	-7.91	5.88	59.20
MR-AGN-20-3:1	3:1	2×10^{-3}	7.46	-0.28	-9.31	5.30	59.01
MR-AGN-20-6:1	6:1	2×10^{-3}	7.22	-0.79	-3.90	4.21	58.77

^{a} AGN feedback efficiency
^{b} $l^{\rm BH,eff} \equiv \log(L_{\rm BH}^{\rm eff}/L_{\rm Edd})$ where $L_{\rm BH,opt}^{\rm eff}$ is the BH luminosity in the optical band after absorption, i.e., as it will be seen from infinity.
The maximum and minimum Eddington rates are listed in column (5) and (6) respectively.
^{c} The fluctuation level of the mass accretion measured following Equation 11 after the final coalescence of black hole.
^{d} Total black hole feedback energy distributed throughout the total simulation time.
^{e} Thermal feedback model with commonly adopted feedback efficiency $\epsilon_f = 5 \times 10^{-3}$ (e.g. Springel, Di Matteo & Hernquist 2005b).
^{f} Our fiducial model with momentum and radiation AGN feedback with modified black hole mass accretion and feedback efficiency
$\epsilon_f = 2 \times 10^{-3}$.
^{g} Our fiducial model only with momentum AGN feedback with modified black hole mass accretion.

curves), to quantitatively show the effect of radiative feedback. We also show the high resolution run with twice the mass resolution for the fiducial model in green curves (High-MR-AGN-20).

Figure 1(a) shows that the inclusion of the AGN feedback in mechanical form reduces the star formation rate before and at the coalescence of the two galaxies at $t \sim 1.5$ Gyr. After the encounter, both AGN feedback models have lower star formation rate compared to the no black hole model (Springel, Di Matteo & Hernquist 2005b). The star formation is more efficiently terminated by the MR-AGN feedback than in Th-AGN feedback as the thermal energy added to the star forming gas particle is radiated away quickly because of the short cooling time. Total amount of stars formed and the total supernova feedback energy distributed during the model evolution for all models are listed in Column (10) and (11) of Table 4. The total amount of stars formed and the corresponding supernovae feedback energy are reduced by 40 percent in MR-AGN-20 compared to No-AGN. High resolution run shows higher late-time star formation rate compared to the fiducial run resulting in 20 percent more total amount of stars formed due to the effective cooling and refueling of the gas from gaseous halo.

Figures 1(b) and (c) show the total black hole accretion rates and the Eddington ratios, respectively. In the Th-AGN-50 model, the black hole mass accretion rate increases rapidly during the encounter and final coalescence. In a short time the black hole grows by an order of magnitude reaches its final mass to within a factor of a few (Figure 1(d)). Af-

terwards, the accretion rates are low with Eddington ratios slowly decreasing from $\dot{M}_{\rm BH}/\dot{M}_{\rm Edd} \sim 10^{-4}$ to 10^{-5}. In MR-AGN-20 model, accretion rates are much more variable with short episodes of efficient accretion even after the black hole coalescence reaching $\dot{M}_{\rm BH}/\dot{M}_{\rm Edd} \geqslant 0.1$ (Figure 1(c)). In order to quantify the fluctuation level of black hole mass accretion for each model, we define a fluctuation parameter $\sigma_{\rm fluc}$ as,

$$\sigma_{\rm fluc}^2 \equiv \left\langle (l_{1\rm Myr} - l_{50\rm Myr})^2 \right\rangle, \tag{11}$$

where $l_{1\rm Myr}$ denotes the logarithmic Eddington ratio of black hole mass accretion measured in time bins of one Myr, and $l_{50\rm Myr}$ is the smoothed Eddington ratio measured in 50 Myr time bins as $l_{50\rm Myr} = \log(\left\langle \dot{M}_{\rm BH} \right\rangle_{\Delta t=50\rm Myr}/\dot{M}_{\rm Edd})$. We determine the global fluctuation level in the Eddington ratio by averaging over all one Myr bins after the black hole merger. The calculated fluctuation parameters $\sigma_{\rm fluc}$ are listed in Column (7) in Table 3. The fluctuation level of mass accretion in MR-AGN-20 is ~ 4.7, which is significantly larger than for all Th-AGN models (~ 0.2). Despite the dramatic differences in the time dependence of the accretion rates (cf. Figure 1(b) and (c)), the final black hole masses in the two cases are quite similar (Figure 1(d)). Including the radiative feedback shows moderate impact on the growth of black hole, reducing the final black hole mass by 20 percent. In the high resolution run we find a slight trend of lower mass accretion rates during the initial passage, but the effects are less than 10 percent.

Table 4. The simulated merger sample: Galaxy properties

Model	Mass Ratio	$\epsilon_{\rm f}$	$\sigma_{\rm bul,f}{}^{a}$ km s^{-1}	$R_{\rm eff}$ kpc	$\log L_{\rm X}{}^{b}$ erg s^{-1}	$\log M_{\rm wind}{}^{c}$ $M_{\odot}$	$\log E_{\rm wind}{}^{c}$ erg	$\log L_{\rm kin}{}^{d}$ erg s^{-1}	$\log M_*{}^{e}$ $M_{\odot}$	$\log E_{\rm SN}{}^{f}$ erg
(1)	(2)	(3)	(4)	(5)	(6)	(7)	(8)	(9)	(10)	(11)
No-AGN	1:1	-	199.9	1.14	39.16	10.03	57.44	41.34	10.30	59.57
Th-AGN-50	1:1	5×10^{-3}	187.6	1.32	39.75	9.53	57.68	41.40	10.23	59.50
Th-AGN-20	1:1	2×10^{-3}	180.7	1.37	38.80	9.42	57.82	41.66	10.22	59.49
Th-AGN-05	1:1	5×10^{-4}	172.7	1.51	38.39	9.40	58.01	42.00	10.18	59.45
MR-AGN-50	1:1	5×10^{-3}	182.4	1.30	39.30	9.31	58.67	42.12	10.18	59.44
MR-AGN-20	1:1	2×10^{-3}	171.8	1.55	38.24	9.29	58.54	42.02	10.09	59.36
M-AGN-20	1:1	2×10^{-3}	160.6	1.72	38.14	9.36	58.43	42.25	10.03	59.30
MR-AGN-05	1:1	5×10^{-4}	155.7	1.97	36.66	9.41	58.65	42.47	10.06	59.33
High-MR-AGN-20^{g}	1:1	2×10^{-3}	184.9	1.35	38.27	9.32	58.59	41.85	10.16	59.43
Th-AGN-50-2:1	2:1	5×10^{-3}	139.9	1.48	41.07	9.34	57.65	39.17	9.97	59.24
Th-AGN-50-3:1	3:1	5×10^{-3}	126.4	1.54	40.84	9.34	57.73	38.59	9.85	59.12
Th-AGN-50-6:1	6:1	5×10^{-3}	120.3	1.52	40.50	9.05	57.40	37.09	9.73	59.00
MR-AGN-20-2:1	2:1	2×10^{-3}	132.5	1.80	36.63	9.46	58.36	41.82	9.79	59.06
MR-AGN-20-3:1	3:1	2×10^{-3}	123.6	1.76	37.48	8.96	58.14	41.52	9.70	58.97
MR-AGN-20-6:1	6:1	2×10^{-3}	119.5	1.58	37.50	8.05	57.81	41.22	9.67	58.94

^{a} Initial value of pre-merger primary galaxy $\sigma_{\rm ini} \sim 105$ km s^{-1}.

^{b} X-ray luminosity measured in 0.3-8 KeV band.

^{c} Total amount of ISM mass lost and wind kinetic energy measured at r =5 kpc from the galactic centre after the final black hole coalescence.

^{d} Mechanical luminosity $L_{\rm kin} \equiv \dot{M}_{\rm wind} v_{\rm wind}^{2}/2$ averaged over 0.2 Gyr by the end of the model evolution.

^{e} Total amount of star formed during the model evolution.

^{f} Total supernova feedback energy distributed during the model evolution.

We now proceed to study the star formation histories and the black hole accretion histories for mergers with varying mass ratios. We ran four mergers with mass ratios of 2:1, 3:1, 4:1 and 6:1 on similar orbits (G13) as the equal mass-merger, adopting the MR-AGN feedback model. In Figure 2, we show the evolution of (a) the resulting star formation rates, (b) the total black hole accretion rates, (c) the Eddington ratios, and (d) the total black hole mass for the four minor mergers as a function of time. Note that we smooth the model outputs shown in Figure 2 with longer time step ($\Delta t = 20$ Myr) than in Figure 1 ($\Delta t = 5$ Myr) to give the overall mean evolution. Almost independent of the progenitor mass-ratio the combined star formation rates are only mildly decreasing from 2 $M_{\odot}$/yr to 1 $M_{\odot}$/yr over 3 Gyrs with only a mild peak in the 2:1 case during the coalescence. The dependence of the mass-ratio is even weaker here than for thermal feedback models (See Figure 6 in Johansson, Naab & Burkert 2009) as we include hot gaseous halos which constantly supply gas (Moster et al. 2011, 2012). A similar weak evolution and weak trend with mass-ratio is found for the the black hole accretion rates and the Eddington ratios (Figure 2 (b) and (c)). In all cases, the black hole accretion rates are variable with the Eddington ratios ranging from 10^{-6} to 0.1 (Note the maximum ratio for equal-mass mergers is about unity) as shown in Figure 2(c). The evolution of the black hole accretion rates are mirrored in the growth of the black hole masses, with the final black hole masses being slightly lower in remnants of higher mass-ratio mergers.

3.2 Properties of the post merger gas outflow

In this section we investigate the physical properties of the gas outflow from the central parts of the galaxies produced by the three feedback models. As detailed before, the energy injection conditions near the black hole in the mechanical and the thermal model are quite different. In the MR-AGN model, gas surrounding the black hole is ejected in a wind with an initial velocity of $\sim 10,000$ km s^{-1} (Ostriker et al. 2010, CONJ12). On the other hand the thermal heating from the accreting black hole in the Th-AGN model drives slow and hot outflows in the vicinity of the black hole as shown in Springel, Di Matteo & Hernquist (2005b).

To parametrize the cumulative mass outflow from the central parts of the merger remnants we measure the fraction of gas mass leaving a central sphere with a fiducial galactocentric radius of $r = 5$ kpc after the final black hole coalescence. We also measure the instantaneous outflow rate and the velocity of the outflowing gas. With this we calculate a corresponding mechanical luminosity as $L_{\rm wind} \equiv \dot{M}_{\rm wind} v_{\rm wind}^{2}/2$, i.e., the kinetic energy carried away by the outflowing gas.

The temporal evolution of the outflowing gas properties (the cumulative outflowing gas mass leaving a central region normalized by the total amount of gas in the central region at the final black hole coalescence, the specific outflow rate, i.e., the rate of gas mass loss normalized by the total amount of gas left at the final black hole coalescence, outflow velocity and mechanical luminosity) after the final black hole coalescence at $t \sim 1.5$ Gyr of the No-AGN
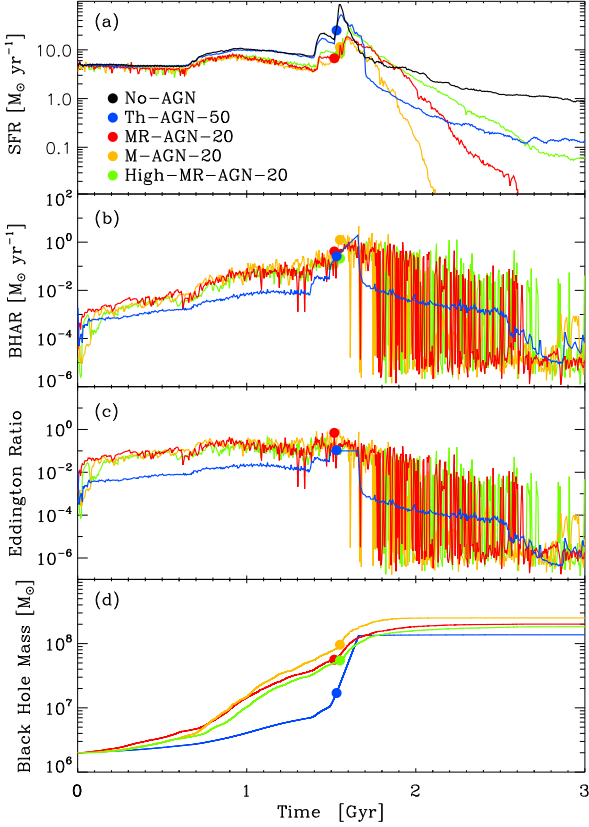
Figure 1. Comparison of the feedback models with a major merger of two galaxies: no AGN (No-AGN, black), thermal feedback (Th-AGN-50, blue), momentum and radiation feedback (MR-AGN-20, red), and momentum feedback (M-AGN-20, orange). Higher resolution ru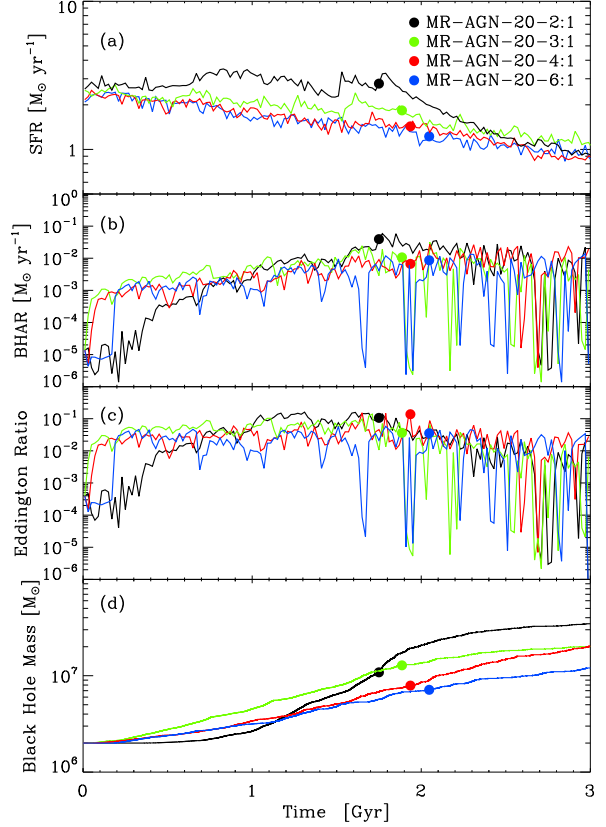n for our fiducial model, High-MR-AGN-20 is shown in green. (a) Evolution of the total star formation rate, (b) the total accretion rate onto the black hole, (c) the Eddington ratio of the mass accretion ($\dot{M}_{\rm BH}/\dot{M}_{\rm Edd}$), and (d) the evolution of the black hole mass are shown as a function of time. The filled circles indicate the time of black hole merger. Note that the model outputs are smoothed identically to have equal time bin $\Delta t = 5$ Myr.

Figure 2. (a) The total star formation rate, (b) the total accretion rate onto the black hole, (c) the Eddington ratio of the mass accretion ($\dot{M}_{\rm BH}/\dot{M}_{\rm Edd}$), and (d) the evolution of the black hole mass as a function of time for 2:1 (black), 3:1 (green), 4:1 (red), and 6:1 (blue) mergers with the mechanical and radiation AGN feedback. The filled circles indicate the time of black hole merger. The model outputs are smoothed identically to have equal time bin $\Delta t = 20$ Myr.

model and our fiducial AGN feedback models Th-AGN-50, MR-AGN-20 and M-AGN-20 are shown in Figure 3.

The MR-AGN-20 model depletes the gas in the central region of the galaxy most effectively and loses the largest fraction of gas after the merger, i.e., ~ 15 percent of gas leaves a central sphere by outflow (Figure 3(a)). The model without black hole also loses the large amount of gas after the merger, primarily driven by the merger induced shock and star formation, but the fraction of outflowing gas mass to the total gas mass within a central sphere is smaller compared to the AGN feedback models.

The corresponding specific outflowing mass loss rates are shown in Figure 3(b). The MR-AGN-20 model has the highest rate, especially after the merger with the timescale for gas depletion by outflow of $\tau_{\rm depletion} \sim 2.9$ Gyr. At later times the specific outflowing mass loss rate for the mechanical AGN model drops and becomes comparable to other models.

The MR-AGN-20 model also shows the highest outflow

velocities of $v_{\rm w} \sim 800 - 1500$ km s^{-1} (Figure 3(c)). These values are comparable to recent observations which indicate outflow velocities in the range of 700 km/s to 3000 km/s (Fischer et al. 2011; Pounds & Vaughan 2011; Sturm et al. 2011; Müller-Sánchez et al. 2011; Rupke & Veilleux 2013). The velocities in the thermal AGN model are much lower and do not exceed the $400 - 500$ km s^{-1} which are comparable to the velocity of the shock heated gas in the No-AGN model.

The mechanical luminosities of the outflowing gas for the three models are shown in Figure 3(d). Overall, Th-AGN-50 has lower mechanical luminosity $L_{\rm wind} \sim 10^{41}$ erg/s, mainly because of its slow outflow velocity. The MR-AGN-20 with momentum feedback has mechanical luminosities a factor of 5-10 higher than the thermal feedback. The total kinetic energy carried away by the winds, i.e., the mechanical luminosities integrated over the simulation time after the merger for the Th-AGN-50 model is $\Delta E_{\rm wind} \sim 1.94 \times 10^{58}$ ergs, while the MR-AGN-20 model deposits $\Delta E_{\rm wind} \sim 6.89 \times 10^{58}$ ergs (3.6 times larger) into the ISM within 1.5 Gyrs. The properties of the outflowing gas of the control run without X-ray radiative heating (M-
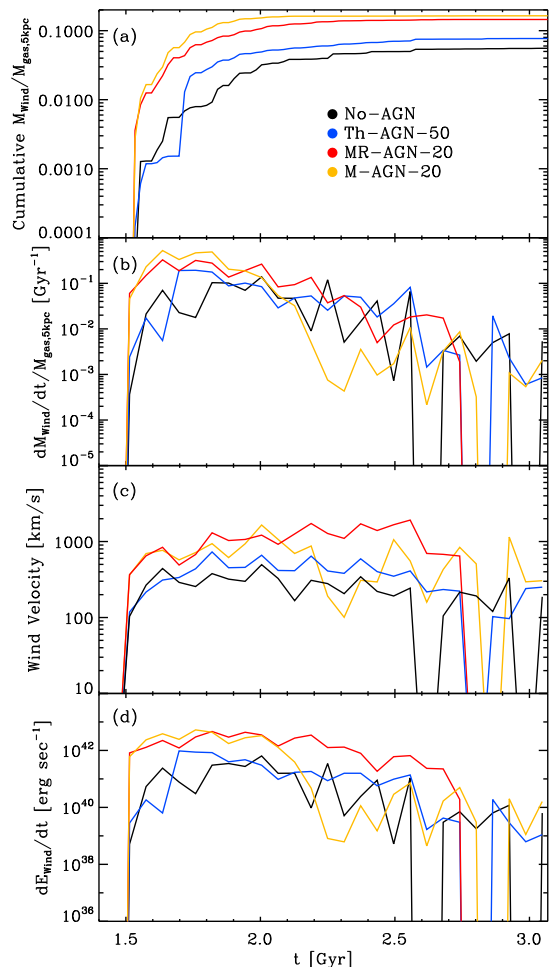
Figure 3. The properties of the outflowing gas in three feedback models: no AGN (No-AGN, black), thermal feedback (Th-AGN-50, blue), momentum and radiation feedback (MR-AGN-20, red), and momentum feedback (M-AGN-20, orange) (a) the fraction of mass depleted by wind within a central sphere with a fiducial galactocentric radius of $r = 5$ kpc after the final black hole coalescence, (b) the specific outflowing mass loss rate, i.e., the rate of gas mass loss normalized by the total amount of gas left in the central region of the galaxy at the final black hole coalescence, (c) outflowing gas velocities and (d) the corresponding mechanical luminosities are shown.

AGN-20) are essentially similar to our fiducial model except for the higher cumulative wind mass. This is due to the higher black hole mass growth in M-AGN-20.

The outflowing gas removed from the central region would propagate to the outer region of the galaxy and increase the kinetic energy of the gas component. Figure 4(a) shows the total kinetic energy of the gas in the outer region of the galaxy ($r > 20$ kpc). In the MR-AGN-20, the bulk of mass and kinetic energy are dissipated by the outflowing gas from the AGN and located in the outer part of the galaxy. The Th-AGN-50 also distributes increased kinetic energy in the outer part, especially right after the final coalescence of the black holes, but the increment is much smaller compared to the MR-AGN model with the AGN-induced winds. The
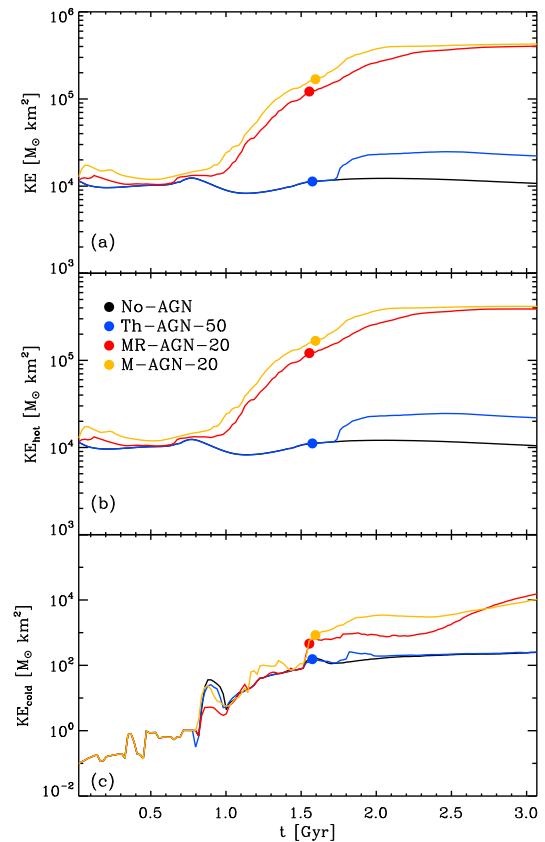
Figure 4. (a) Total kinetic energy of the gas, (b) the kinetic energy of the warm gas with $T > 10^{4.5}$ K, and (c) the kinetic energy of the cold gas with $T < 10^{4.5}$ K in the outer region of the galaxy ($r > 20$ kpc) are shown for the three feedback models: no AGN (No-AGN, black), thermal feedback (Th-AGN-50, blue), momentum and radiation feedback (MR-AGN-20, red), and momentum feedback (M-AGN-20, orange).

total kinetic energy in the outflow, as seen in Figure 4(a), is a factor of 20 higher in the MR-AGN then in the Th-AGN case. While the kinetic energy in the outer region of the galaxy is dominated by the warm component with the temperature $T > 10^{4.5}$ K, as shown in Figure 4(b), the MR-AGN model also sweeps up and drives out cold gas increasing the kinetic energy of the cold component with $T < 10^{4.5}$ K (see Figure 4(c)). The Th-AGN model, however, has negligible effect on the cold gas component within the framework of the standard multiphase star formation model as pointed out by Barai et al. (2014). We find a slight trend of higher kinetic energy during the initial passage in the mechanical feedback run without X-ray heating (M-AGN-20) but this is originated from the different black hole mass accretion history, higher black hole mass and black hole accretion rate in M-AGN-20.
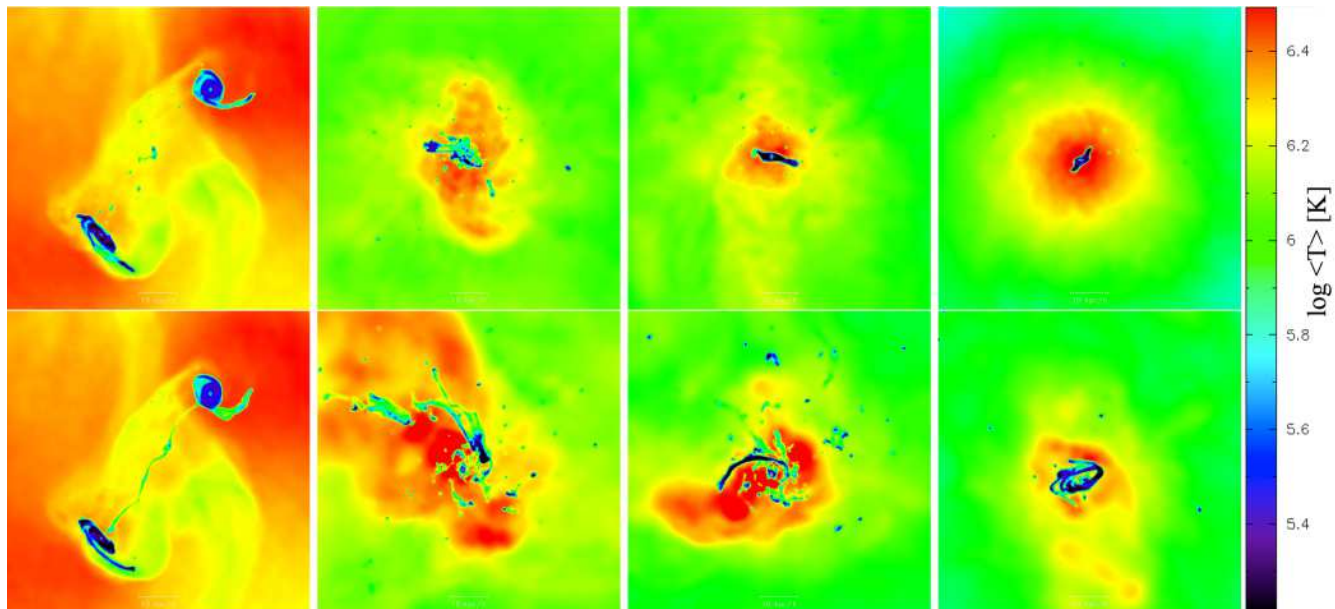
Figure 5. A sequence of snapshots of the mass-weighted gas temperature during a major merger of two models: Th-AGN-50 (top panels) and MR-AGN-20 (bottom panels). The snapshots after the first close passage of the two galaxies at $t = 0.92$ Gyr, right after the galaxies and black holes merge at $t = 1.78$ Gyr, and afterwards at $t = 2.0$, 2.64 Gyr are shown from left to right. The images are 80 kpc on a side and redder color indicates a higher temperature.

4   PROPERTIES OF MERGED GALAXIES

4.1   Distribution of gas during the merger

Figure 5 shows a sequence of snapshots of the mass-weighted average gas temperature along the line of sight during a merger of Th-AGN-50 (top) and MR-AGN-20 (bottom). The snapshots show the first close passage at $t = 0.92$ Gyr, the time right after the final coalescence at $t = 1.78$ Gyr and afterwards at $t = 2.0$, and 2.64 Gyr from left to right. In Th-AGN-50 model, the heated gas expands from the central region and forms a hot gaseous halo by the end of the simulation while the MR-AGN-20 model show less hot gas. In both simulations we found tidal condensations which consist of cold dense gas but there are significantly more materials at large distance in dense cold blobs in MR-AGN-20 model.

4.2   X-ray properties

We compare the evolution of hot gas and X-ray emission of the No-AGN and two feedback models. Following Cen et al. (1995), we calculate the X-ray luminosity due to bremsstrahlung radiation as well as line emissions of all the species using the computed X-ray emissivity spectra tables, kindly made available to us by R. Cen. The emission rates from H, He and metals are given separately assuming that the gas is in ionization equilibrium and optically thin. We calculate the total emissivity by summing the emission rates of the all components weighted by the relative abundance assuming solar abundance. Then we compute the integrated luminosity for 0.3-8 keV band using the computed total emissivity. We assume that the central region of the galaxy remains obscured because of the large column density of intervening gas and dust, therefore we only include the X-ray contribution from hot and diffuse gas par-
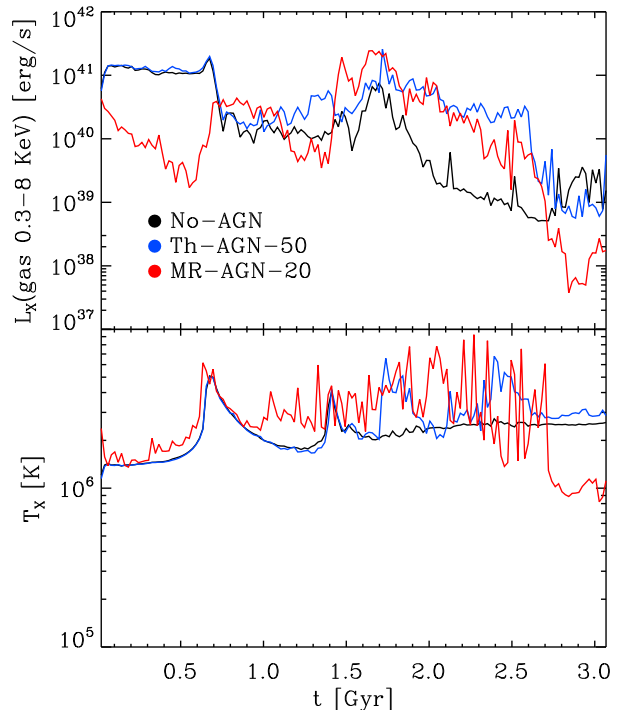

Figure 6. Galactic X-ray coronal luminosity L_X (top), and the X-ray luminosity-weighted temperature of the hot and diffuse gas component with a temperature of $T \geqslant 10^6$ K, and a density $\rho \leqslant 3.16 \times 10^{-3} M_\odot$ pc^{-3} (bottom).

ticles. Following Cox et al. (2006), we define the 'hot and diffuse gas' with a temperature of $T \geqslant 10^6$ K, and a density $\rho \leqslant 3.16 \times 10^{-3} M_\odot$pc^{-3}, which corresponds to the criti-

cal density for star formation, so effectively we exclude star forming gas.

Figure 6 shows the X-ray luminosities for photons with energies of 0.3-8 keV for No-AGN, Th-AGN-50 and MR-AGN-20 as a function of time. Before the galaxy interaction, the majority of the X-ray emission is produced by pre-existing hot halo gas, but in the MR-AGN-20 model, the high velocity gas outflow by AGN momentum feedback effectively drives out the gaseous halo, lowering the X-ray luminosity. The system begins to emit more X-rays at the first interaction of galaxies at ~ 0.7 Gyr, in shocks that lie directly between the two discs. During the galaxy interaction, the majority of the X-ray emission is produced by shock-heated gas, as Th-AGN-50 shows very similar X-ray luminosity compared to No-AGN model. By the time of the final coalescence, $t \sim 1.5$ Gyr, however, the X-ray luminosity increases in both AGN models. In the Th-AGN-50 model, the X-ray luminosity decreases much more slowly as the black hole keeps depositing a significant amount of thermal energy. On the other hand, in the mechanical feedback model, the hot gas in the remnant is driven outwards more effectively and the X-ray luminosity decreases quickly. The final X-ray emission of the Th-AGN-50 is higher (1.6×10^{39} erg s^{-1}) compared with the observed luminosity (0.3-8 KeV) of the galaxies with corresponding velocity dispersions. The MR-AGN-20 model, however, results in lower X-ray luminosity (9.8×10^{37} erg s^{-1}) that better reproduces observed values (e.g., Boroson, Kim & Fabbiano 2011).

4.3 Galaxy-black hole Scaling relation

We now proceed with a detailed analysis of the effect of the black hole feedback prescription and feedback efficiency on the final mass of black holes and the corresponding stellar velocity dispersions in the merger remnants. We simulate equal-mass mergers with different feedback efficiencies and unequal-mass mergers with the adopted fiducial feedback efficiencies ($\epsilon_f = 5 \times 10^{-3}$ for Th-AGN and $\epsilon_f = 2 \times 10^{-3}$ for MR-AGN) for both feedback models and compare them with the observed $M_{BH} - \sigma$ relation. We calculate the final black hole mass together with the mass-weighted line-of-sight stellar velocity dispersion σ measured from all stellar particles within the projected half-mass radius r_e. The feedback efficiency has a strong effect on the final black hole mass of the merger remnant in both feedback models, with the higher efficiency producing lower black hole masses. For the final stellar velocity dispersion on the other hand, the effect of feedback efficiency is less pronounced. The simulated Th-AGN-50 and MR-AGN-20 results are overplotted on the observed $M_{BH} - \sigma$ by Tremaine et al. (2002) and McConnell & Ma (2013) as shown in Figure 7(a). In unequal-mass merger cases, MR-AGN-20 models evolve close to the observed $M_{BH} - \sigma$ relation while Th-AGN-50 models result in lower black hole mass compared to the observed relation.

We show the X-ray luminosity of the hot gas against the stellar velocity dispersion σ in Figure 7(b). Observationally all galaxies with a shallow potential well with $\sigma < 200$ km s^{-1} seem to have only a small amount of hot gas with $L_X < 10^{40}$ erg s^{-1} (Boroson, Kim & Fabbiano 2011). Observed L_X(gas) is correlated with σ, although not as strongly as the $M_{BH} - \sigma$ relation. The effect of the black hole feedback prescription and feedback efficiency on the fi-

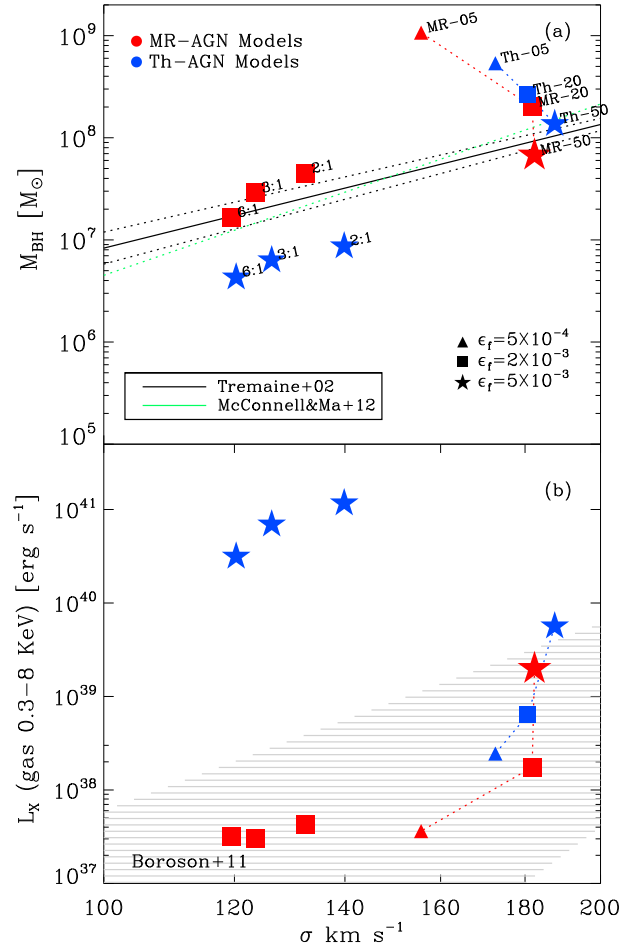**Figure 7.** (a) $M_{BH} - \sigma$ relation of the two feedback models. The blue symbols show Th-AGN models and red symbols show the MR-AGN models. Different symbols indicate the different feedback efficiencies. The merger progenitor mass ratios are indicated for the minor merger cases. The black and green lines show the observed relation with errors by Tremaine et al. (2002) and by McConnell & Ma (2013). (b) X-ray luminosity of the hot gas is plotted against stellar velocity dispersion σ. Observed relation (hatched region) is from Boroson et al. (2011).

nal stellar velocity dispersion is minor resulting in typically $160 < \sigma < 190$ km s^{-1}, however the effect on the X-ray luminosity is significant. Adopting higher feedback efficiency produces higher X-ray luminosity. Th-AGN-50 produces X-ray luminosities that are higher for the corresponding velocity dispersions. We show that reducing the feedback efficiency to $\epsilon_f = 5 \times 10^{-4}$ produces X-ray luminosity within the observed range, but the resulting final black hole mass is factor of 20 larger than the one for its corresponding σ in the thermal feedback cases. On the other hand, MR-AGN models result in lower X-ray luminosity compared to the Th-AGN models, and our proposed model MR-AGN-20 reproduces both the observed $L_X - \sigma$ relation and $M_{BH} - \sigma$ relation. In case of minor mergers, all Th-AGN models show excessive X-ray luminosity compared to the observed range. The physical reason for the different results is easy to understand. The MR-AGN models tends to expand the gaseous
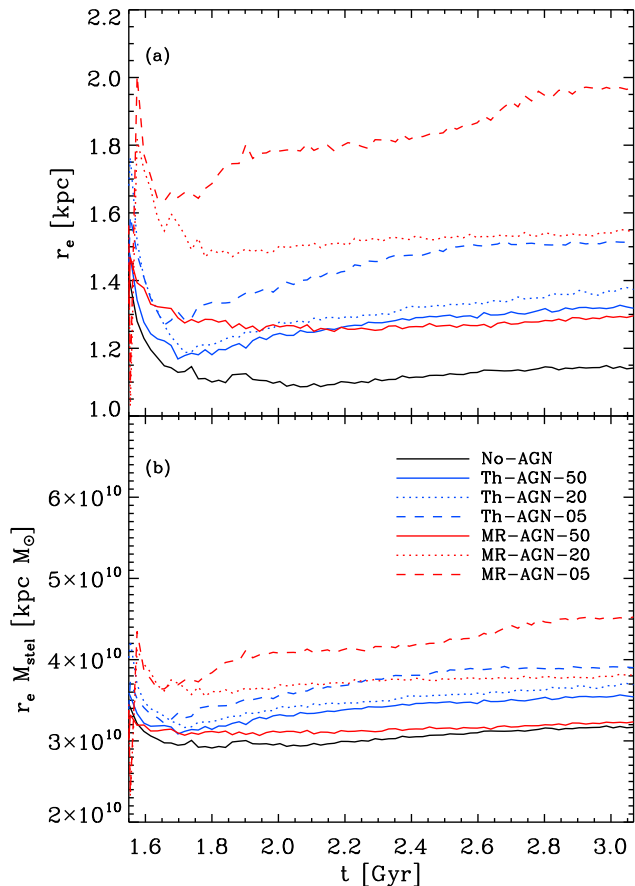
Figure 8. (a) Evolution of the effective radius, and (b) the adiabatic invariant for two feedback models.

halo more than the Th-AGN, thus reducing the gas density and the thermal X-ray luminosity.

4.4   Galaxy Size

Observations have shown that quiescent massive galaxies at high redshift are much more compact than the local galaxies with the comparable mass and they have grown in physical size from $z \sim 1$ to $z \sim 0$ (e.g., Ferguson et al. 2004; Trujillo et al. 2004; Longhetti et al. 2007; Toft et al. 2007; Trujillo et al. 2007; Cimatti et al. 2008; van Dokkum et al. 2008; Damjanov et al. 2009). Some physical explanations have been suggested to explain this growth in size while avoiding the overproduction of present-day massive galaxies. Minor mergers involving lower mass galaxies has been proposed as one of the explanations, as they can produce efficient size growth (Naab, Johansson & Ostriker 2009). Hopkins et al. (2010) considered the various proposed channels for observed size evolution, and concluded that minor dry mergers are the "prime candidate" for explaining the majority of the observed sized growth, though other channels including adiabatic expansion due to mass loss from stellar winds should play a non-negligible role. However, the accretion of satellite stellar systems in minor mergers mainly contribute to the mass growth in the outer parts of elliptical galaxies (Oser et al. 2012;

Hilz, Naab & Ostriker 2013) and in this picture a factor of two decrease in central densities observed by Abraham et al. (2007); van Dokkum et al. (2008); Szomoru et al. (2010) cannot be fully explained (cf. Hilz, Naab & Ostriker 2013). Other candidates include AGN feedback-driven star formation (Ishibashi, Fabian & Canning 2013) and secular processes such as adiabatic expansion driven by the expulsion of a substantial fraction of the gas out of the galaxy by stellar winds and/or strong AGN feedback (Fan et al. 2008, 2010). In the recent studies (Martizzi et al. 2012; Dubois et al. 2013), it is shown that the galaxies simulated with AGN feedback is more extended due to the AGN feedback induced gas expulsion compared to the no-AGN cases.

In this section, we test the possible contribution of the *puffing-up* process by the AGN mechanical feedback prescriptions, which have very different timescales for the AGN-driven winds. We also check whether the size increase by the AGN feedback induced mass loss which can account for the observed evolution is permitted by observational constraints on $M_{\rm BH} - \sigma$.

The effect of the mass loss on the structure and dynamics of a stellar system depends on the amount of mass loss and on the timescale of ejection. The puffing up of a virialized stellar system by rapid mass loss is a well-known phenomenon, extensively studied both analytically and through numerical simulations, with reference to galaxies (Biermann & Shapiro 1979), and to star clusters (Hills 1980; Ragone-Figueroa & Granato 2011). Adiabatic expansion can be also caused by much slower mass loss, for example, by stellar winds. If we define the fraction of changes in radius and in mass respectively as $\delta_r \equiv (r_1 - r_0)/r_0$ and $\delta_m \equiv (m_1 - m_0)/m_0$ where m_0 and m_1 are the initial and final masses and r_0 and r_1 are the initial and final radii, we have

$$\delta_r = -\frac{\delta_m}{2\delta_m + 1}, \tag{12}$$

when we have a rapid mass loss with a shorter ejection timescale than the dynamical timescale. In this rapid mass loss case, when about a half of total mass is lost ($\delta_m \sim -0.5$), the radius expansion can be significantly larger than in adiabatic changes, when the mass loss occurs on a timescale longer than the dynamical timescale. In this case, the expansion proceeds at a rate proportional to the mass loss rate ($\delta_r = -\delta_m/(\delta_m + 1)$).

In the top panel of Figure 8, we show the temporal evolution of half-mass radii of the simulated galaxies of No-AGN and two AGN feedback models: Th-AGN and MR-AGN with three feedback efficiencies respectively. After the final galactic nuclei coalesce at $t \sim 1.5$ Gyr, MR-AGN-05 model has a large and continuous increase of the galaxy size, with the half-mass radius increasing by a factor of 1.25. MR-AGN models tend to have larger increment in size compared to the Th-AGN models. As discussed above, the momentum-based mechanical AGN feedback model can more rapidly and impulsively remove a large amount of cold gas from the baryon-dominated central regions of the galaxies. It can trigger a puffing up of the central region of the stellar component while the dark matter halo extending far beyond the stellar distribution stabilizes the system and prevents its total disruption. However, the MR-AGN-05 model which shows the considerable size increase has much larger black
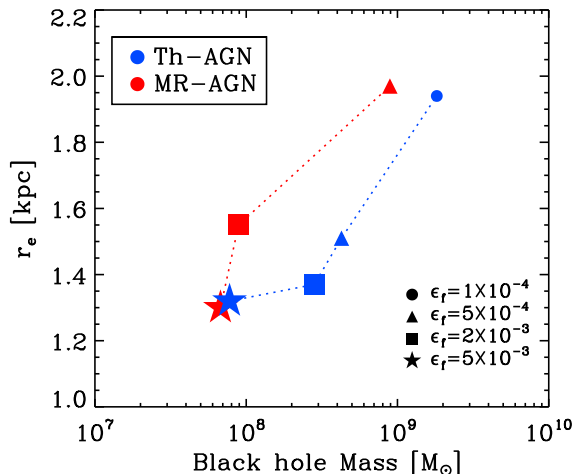
Figure 9. Galaxy size evolution of two feedback models, Th-AGN (blue) and MR-AGN (red), as a function of total black hole growth. Three models are shown for MR-AGN, with the feedback efficiency $\epsilon_f = 5 \times 10^{-3}$, 2×10^{-3} and 5×10^{-4}, with different symbols for the respective efficiencies. Th-AGN models with the same efficiency are shown along with the additional model of $\epsilon_f = 1 \times 10^{-4}$ which has high enough mass growth in black hole comparable to MR-AGN-05.

Figure 10. Evolution of gas mass enclosed within central 2 kpc radius (top) and stellar mass enclosed within central 1 kpc radius (bottom).

hole mass growth with $M_{\rm BH} > 10^9 M_\odot$, which is inconsistent with the observed $M_{\rm BH} - \sigma$ relation. For MR-AGN-20 model consistent with the $M_{\rm BH} - \sigma$ relation, the size increase is negligible. Adiabatic expansion due to mass loss from AGN feedback plays a minor role for galaxy size growth as found in Hopkins et al. (2010).

In the bottom panel of Figure 8, we show the adiabatic invariant of the stellar component of the system. In most models, the adiabatic invariant shows minor increment, while MR-AGN-05 with the largest size increase shows the largest increase in the adiabatic invariant. The puffing-up process of the mechanical feedback models is non-adiabatic, and more efficient than the thermal feedback models following Equation 12.

We compare the effect of two AGN feedback models on the galaxy size as a function of total black hole mass growth in Figure 9. We show 3 models with MR-AGN feedback: MR-AGN-50, MR-AGN-20, and MR-AGN-05. In case of Th-AGN feedback models, we show the results with the identical feedback efficiencies, and additionally add one more model with the $\epsilon_f = 1 \times 10^{-4}$ which shows the large enough mass growth in black hole comparable to MR-AGN-05. For the same mass growth in black hole, MR-AGN models have bigger effective radius than Th-AGN models as rapid mass loss effectively induces the puffing-up process. As before, the models with the lower AGN feedback efficiency show the considerable size increase but have much higher black hole mass growth, inconsistent with the observed $M_{\rm BH} - \sigma$ relation. Adiabatic expansion requires significant amount of mass loss by outflowing gas, thus requires a large black hole mass growth to be the explanation for the observed size evolution.
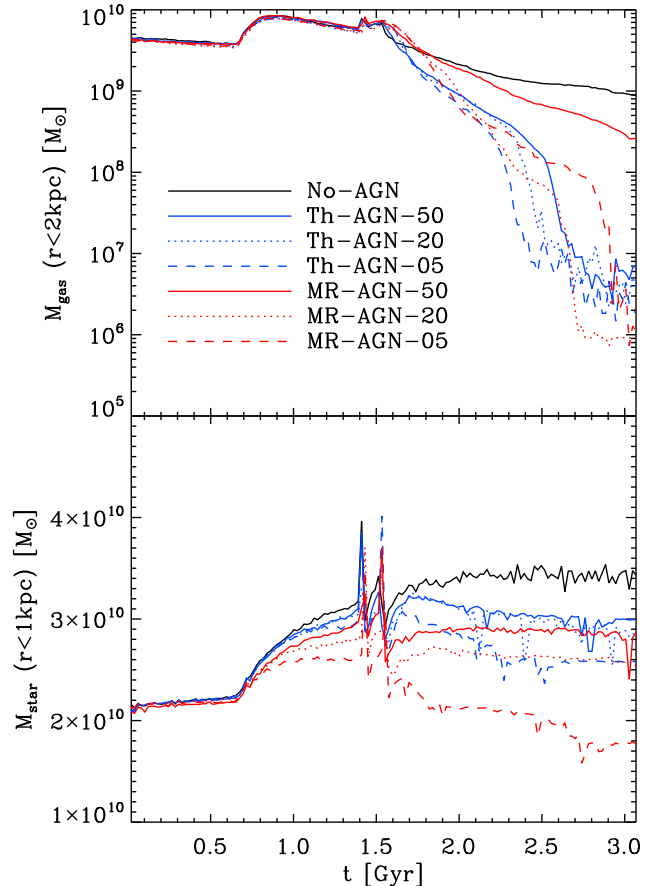
4.5 Central density

Figure 10 shows the evolution of the gas and the stellar masses contained within a fixed radius (1 kpc) in major merger simulations. The amount of gas in the central region of the galaxies decreases due to the star formation, black hole mass accretion and the outflowing gas by the AGN feedback in both feedback models. The model MR-AGN-50, which has a smallest mass growth in black hole, shows the smallest decrease in gas within 2 kpc radius. In case of the stellar mass, both feedback models have lower central stellar density compared to No-AGN model mainly due to the less gas remaining in the central region of the galaxy, but the difference tends to be larger in MR-AGN models. Compared to the No-AGN model, Th-AGN-50 has 13 percent less stellar mass and MR-AGN-20 has 25 percent less stellar mass within 1 kpc radius. The central densities show little decrease after the merger despite the fact that the gas is thrown out by AGN feedback in most models. However, in case of MR-AGN-05 which shows the largest increase in galaxy size, the central density decreases by 30 percent after the merger. As before, the quasar activity can lower the central stellar density of the galaxy, but only when it has enough black hole mass growth and a corresponding large amount of outflowing gas. However, the required black hole mass growth to explain

the recent observations of the mild decrease of central stellar mass in elliptical galaxies (e.g. Milosavljević & Merritt 2001; Szomoru et al. 2010; Saracco, Gargiulo & Longhetti 2012; van de Sande et al. 2013) is inconsistent with the observed $M_{BH} - \sigma$ relation.

5   SUMMARY

We have investigated the effects of radiative and momentum-based mechanical AGN feedback on the gas flow in galaxy mergers, with the aid of three-dimensional SPH simulations. Our numerical black hole model incorporates both radiative and mechanical AGN feedback and renders a physically more accurate picture of how a galaxy and its embedded black hole evolve under each others influence, providing a powerful tool in understanding the coevolution of black holes and galaxies. Our main results are as follows:

1. *Self-regulated black hole growth.* We show that our AGN feedback treatment is an effective mechanism for halting further growth of the black hole once it has reached a critical size for the gravitational potential of the bulge. We show the successful treatment of the mechanical and radiation feedback in recovering the observed $M_{BH} - \sigma$ relationship between the black hole mass and the galaxy velocity dispersion with the adopted set of parameters, the initial wind velocity $v_w = 10,000$ km s^{-1} and the feedback efficiency $\epsilon_f = 2 \times 10^{-3}$. This was also obtained in the previous thermal feedback treatments (e.g. Di Matteo, Springel & Hernquist 2005; Springel, Di Matteo & Hernquist 2005b) and remains as a strong argument in helping to understand the observed physical relation between black hole and galactic properties.

2. *Large fluctuation level in black hole mass accretion.* In the mechanical feedback model, the fluctuation level in black hole mass accretion, and therefore also in radiant output, is significantly greater than the thermal feedback prescription. Episodic accretion is the norm with bolometric luminosity fluctuating between $\sim 10^{-1}$ and 10^{-6} of L_{Edd} during merger events.

3. *Galactic outflow.* We show that our feedback model can drive large-scale galactic outflows, which unbind a significant fraction of the gas of the host galaxy. The AGN-driven winds found in this study provide a promising explanation for the moderate velocity outflows observed in some post-starburst galaxies and for the narrow-absorption line winds with $v \sim 500 - 1500$ km s^{-1} seen in local quasars. This behaviour is consistent with the recent founding by Debuhr, Quataert & Ma (2012) who also use a momentum based feedback implementation. Outflowing kinetic energy is 20 times larger in the mechanical feedback models than in the thermal feedback models which show negligible effect on gas properties due to the instantaneous cooling of the thermal energy deposited to the star forming gas in the multiphase star formation model. The mechanical feedback models will have a corresponding larger effect on the surrounding intergalactic medium (e.g., Fabian et al. 2000).

4. *X-ray luminosity from hot gas consistent with observations.* We show that the thermal feedback model with the feedback efficiency of the standard value $\epsilon_f = 5 \times 10^{-3}$ appears to produce X-ray luminosities that are too high for their corresponding velocity dispersions. On the other hand, our fiducial model with mechanical and radiative feedback

prescription spreads the halo gas over a larger volume and results in lower X-ray luminosity from the hot gaseous halo compared to the thermal feedback, and our proposed model with $\epsilon_f = 2.0 \times 10^{-3}$ reproduces observed $L_X - \sigma$ relation and $M_{BH} - \sigma$ relation simultaneously.

5. *The effects of AGN feedback driven mass loss on the size and central density of the host galaxy.* We show that AGN-driven mass loss can moderately increase the galaxy size and decrease the central density. However, as noted in Section 4.4, the required black hole mass growth to fully account for the observed galaxy size evolution is much larger than that observed. Given observational constraints on $M_{BH} - \sigma$ relation, the effect of the mass loss driven by AGN feedback on galaxy size is moderate with the adopted set of parameters.

REFERENCES

Abraham R. G. et al., 2007, ApJ, 669, 184
Aller M. C., Richstone D. O., 2007, ApJ, 665, 120
Anderson M. E., Bregman J. N., 2011, ApJ, 737, 22
Anderson M. E., Bregman J. N., Dai X., 2013, ApJ, 762, 106
Barai P., Viel M., Murante G., Gaspari M., Borgani S., 2014, MNRAS, 437, 1456
Bédorf J., Portegies Zwart S., 2013, MNRAS, 431, 767
Biermann P., Shapiro S. L., 1979, ApJ, 230, L33
Bondi H., 1952, MNRAS, 112, 195
Bondi H., Hoyle F., 1944, MNRAS, 104, 273
Booth C. M., Schaye J., 2009, MNRAS, 398, 53
Booth C. M., Schaye J., 2011, MNRAS, 413, 1158
Boroson B., Kim D.-W., Fabbiano G., 2011, ApJ, 729, 12
Broderick A. E., Chang P., Pfrommer C., 2012, ApJ, 752, 22
Cavaliere A., Fusco-Femiano R., 1976, A&A, 49, 137
Cen R., Kang H., Ostriker J. P., Ryu D., 1995, ApJ, 451, 436
Choi E., Ostriker J. P., Naab T., Johansson P. H., 2012, ApJ, 754, 125
Cimatti A. et al., 2008, A&A, 482, 21
Ciotti L., Ostriker J. P., 2007, ApJ, 665, 1038
Ciotti L., Ostriker J. P., Proga D., 2009, ApJ, 699, 89
Ciotti L., Ostriker J. P., Proga D., 2010, ApJ, 717, 708

Cox T. J., Di Matteo T., Hernquist L., Hopkins P. F., Robertson B., Springel V., 2006, ApJ, 643, 692

Crain R. A., McCarthy I. G., Frenk C. S., Theuns T., Schaye J., 2010, MNRAS, 407, 1403

Crain R. A., McCarthy I. G., Schaye J., Theuns T., Frenk C. S., 2013, MNRAS, 432, 3005

Crenshaw D. M., Kraemer S. B., George I. M., 2003, ARA&A, 41, 117

Dalla Vecchia C., Bower R. G., Theuns T., Balogh M. L., Mazzotta P., Frenk C. S., 2004, MNRAS, 355, 995

Dalla Vecchia C., Schaye J., 2012, MNRAS, 426, 140

Damjanov I. et al., 2009, ApJ, 695, 101

Debuhr J., Quataert E., Ma C.-P., 2012, MNRAS, 420, 2221

Debuhr J., Quataert E., Ma C.-P., Hopkins P., 2010, MNRAS, 406, L55

Dehnen W., 2001, MNRAS, 324, 273

Di Matteo T., Springel V., Hernquist L., 2005, Nature, 433, 604

Dressler A., 1989, in IAU Symposium, Vol. 134, Active Galactic Nuclei, Osterbrock D. E., Miller J. S., eds., p. 217

Dubois Y., Devriendt J., Slyz A., Teyssier R., 2012, MNRAS, 420, 2662

Dubois Y., Gavazzi R., Peirani S., Silk J., 2013, MNRAS

Dunn J. P. et al., 2010, ApJ, 709, 611

Eke V. R., Navarro J. F., Frenk C. S., 1998, ApJ, 503, 569

Fabian A. C. et al., 2000, MNRAS, 318, L65

Fan L., Lapi A., Bressan A., Bernardi M., De Zotti G., Danese L., 2010, ApJ, 718, 1460

Fan L., Lapi A., De Zotti G., Danese L., 2008, ApJ, 689, L101

Ferguson H. C. et al., 2004, ApJ, 600, L107

Fischer T. C., Crenshaw D. M., Kraemer S. B., Schmitt H. R., Mushotsky R. F., Dunn J. P., 2011, ApJ, 727, 71

Gaspari M., Brighenti F., Ruszkowski M., 2013, Astronomische Nachrichten, 334, 394

Gaspari M., Brighenti F., Temi P., 2012, MNRAS, 424, 190

Gaspari M., Ruszkowski M., Oh S. P., 2013, MNRAS, 432, 3401

Gebhardt K. et al., 2000, ApJ, 539, L13

Gültekin K. et al., 2009, ApJ, 698, 198

Guo F., Mathews W. G., 2010, ApJ, 712, 1311

Haardt F., Madau P., 1996, ApJ, 461, 20

Hernquist L., 1990, ApJ, 356, 359

Hills J. G., 1980, ApJ, 235, 986

Hilz M., Naab T., Ostriker J. P., 2013, MNRAS, 429, 2924

Hilz M., Naab T., Ostriker J. P., Thomas J., Burkert A., Jesseit R., 2012, MNRAS, 425, 3119

Hopkins P. F., Bundy K., Hernquist L., Wuyts S., Cox T. J., 2010, MNRAS, 401, 1099

Hopkins P. F., Hernquist L., Cox T. J., Di Matteo T., Martini P., Robertson B., Springel V., 2005, ApJ, 630, 705

Hoyle F., Lyttleton R. A., 1939, Proceedings of the Cambridge Philosophical Society, 34, 405

Ishibashi W., Fabian A. C., Canning R. E. A., 2013, MNRAS, 431, 2350

Johansson P. H., Burkert A., Naab T., 2009, ApJ, 707, L184

Johansson P. H., Naab T., Burkert A., 2009, ApJ, 690, 802

Johansson P. H., Naab T., Ostriker J. P., 2012, ApJ, 754, 115

Jones C., Forman W., 1984, ApJ, 276, 38

Katz N., Weinberg D. H., Hernquist L., 1996, ApJS, 105, 19

Kim J.-h., Wise J. H., Alvarez M. A., Abel T., 2011, ApJ, 738, 54

Kormendy J., 1993, in The Nearest Active Galaxies, Beckman J., Colina L., Netzer H., eds., pp. 197–218

Li J.-T., Wang Q. D., 2013, MNRAS, 428, 2085

Longhetti M. et al., 2007, MNRAS, 374, 614

Lynden-Bell D., 1969, Nature, 223, 690

Magorrian J. et al., 1998, AJ, 115, 2285

Makino N., Sasaki S., Suto Y., 1998, ApJ, 497, 555

Marconi A., Hunt L. K., 2003, ApJ, 589, L21

Martizzi D., Teyssier R., Moore B., Wentz T., 2012, MNRAS, 422, 3081

McConnell N. J., Ma C.-P., 2013, ApJ, 764, 184

McKee C. F., Ostriker J. P., 1977, ApJ, 218, 148

Milosavljević M., Merritt D., 2001, ApJ, 563, 34

Mo H. J., Mao S., White S. D. M., 1998, MNRAS, 295, 319

Moe M., Arav N., Bautista M. A., Korista K. T., 2009, ApJ, 706, 525

Monaghan J. J., 1992, ARA&A, 30, 543

Moster B. P., Macciò A. V., Somerville R. S., Naab T., Cox T. J., 2011, MNRAS, 415, 3750

Moster B. P., Macciò A. V., Somerville R. S., Naab T., Cox T. J., 2012, MNRAS, 423, 2045

Müller-Sánchez F., Prieto M. A., Hicks E. K. S., Vives-Arias H., Davies R. I., Malkan M., Tacconi L. J., Genzel R., 2011, ApJ, 739, 69

Naab T., Burkert A., 2003, ApJ, 597, 893

Naab T., Johansson P. H., Ostriker J. P., 2009, ApJ, 699, L178

Navarro J. F., Frenk C. S., White S. D. M., 1995, MNRAS, 275, 720

Nayakshin S., Power C., 2010, MNRAS, 402, 789

Newman A. B., Ellis R. S., Bundy K., Treu T., 2012, ApJ, 746, 162

Newton R. D. A., Kay S. T., 2013, ArXiv e-prints

Nipoti C., Treu T., Leauthaud A., Bundy K., Newman A. B., Auger M. W., 2012, MNRAS, 422, 1714

Novak G. S., Ostriker J. P., Ciotti L., 2011, ApJ, 737, 26

Omma H., Binney J., Bryan G., Slyz A., 2004, MNRAS, 348, 1105

Oogi T., Habe A., 2013, MNRAS, 428, 641

Oser L., Naab T., Ostriker J. P., Johansson P. H., 2012, ApJ, 744, 63

Ostriker J. P., Choi E., Ciotti L., Novak G. S., Proga D., 2010, ApJ, 722, 642

Pfrommer C., Chang P., Broderick A. E., 2012, ApJ, 752, 24

Pounds K. A., Vaughan S., 2011, MNRAS, 413, 1251

Proga D., Kallman T. R., 2004, ApJ, 616, 688

Puchwein E., Springel V., 2013, MNRAS, 428, 2966

Ragone-Figueroa C., Granato G. L., 2011, MNRAS, 414, 3690

Rees M. J., 1984, ARA&A, 22, 471

Rupke D. S. N., Veilleux S., 2013, ApJ, 768, 75

Saracco P., Gargiulo A., Longhetti M., 2012, MNRAS, 422, 3107

Sazonov S. Y., Ostriker J. P., Ciotti L., Sunyaev R. A., 2005, MNRAS, 358, 168

Shakura N. I., Sunyaev R. A., 1973, A&A, 24, 337

Sijacki D., Pfrommer C., Springel V., Enßlin T. A., 2008, MNRAS, 387, 1403

Sijacki D., Springel V., Di Matteo T., Hernquist L., 2007, MNRAS, 380, 877

Sijacki D., Springel V., Haehnelt M. G., 2009, MNRAS, 400, 100

Springel V., 2005, MNRAS, 364, 1105

Springel V., Di Matteo T., Hernquist L., 2005a, ApJ, 620, L79

Springel V., Di Matteo T., Hernquist L., 2005b, MNRAS, 361, 776

Springel V., Hernquist L., 2003, MNRAS, 339, 289

Sturm E. et al., 2011, ApJ, 733, L16

Szomoru D. et al., 2010, ApJ, 714, L244

Teyssier R., Moore B., Martizzi D., Dubois Y., Mayer L., 2011, MNRAS, 414, 195

Toft S., Rasmussen J., Sommer-Larsen J., Pedersen K., 2002, MNRAS, 335, 799

Toft S. et al., 2007, ApJ, 671, 285

Tremaine S. et al., 2002, ApJ, 574, 740

Trujillo I., Conselice C. J., Bundy K., Cooper M. C., Eisenhardt P., Ellis R. S., 2007, MNRAS, 382, 109

Trujillo I. et al., 2004, ApJ, 604, 521

van de Sande J. et al., 2013, ApJ, 771, 85

van Dokkum P. G. et al., 2008, ApJ, 677, L5